Available online at www.sciencedirect.com
SCIENCE DIRECT®
Optics Communications 225 (2003) 393–402
OPTICS COMMUNICATIONS
www.elsevier.com/locate/optcom

Three-frequency chaotic instability in soft-aperture Kerr-lens mode-locked laser around 1/3-degenerate cavity configuration

Ja-Hon Lin, Wen-Feng Hsieh *

Institute of Electro-Optical Engineering, National Chiao Tung University, 1001 Tahsueh Rd., Hsinchu 30050, Taiwan

Received 30 August 2002; received in revised form 16 January 2003; accepted 1 July 2003

Abstract

The quasi-periodic route to chaos from a three-frequency interaction was experimentally observed when the soft-aperture Kerr-lens mode-locked Ti:sapphire laser was operated in a cavity configuration that was around 1/3-degenerate, with non-zero group velocity dispersion. When the pump beam was smaller than the cold cavity beam, the laser oscillated among three frequencies, resulting in the modulation of phase-locked longitudinal modes. Increasing the pump power caused the nonlinear interaction of the three frequencies to induce a combination tones due to nonlinear gain and Kerr nonlinearity. Further secondary beating of these combinations tones at even higher pumping caused the system to become chaotic. Starting from the period-3 pulses in the 1/3-degenerate configuration, the quasi-periodic route to chaos was also observed when the configuration was tuned slightly away from degeneracy.
© 2003 Elsevier B.V. All rights reserved.

1. Introduction

Since the self-mode-locked Ti:sapphire laser was reported [1] in 1991, it has become the most important tool for generating ultra-short optical pulses. Early studies applied many theories to the design of the cavity for generating a Kerr-lens mode-locked (KLM) laser [2–4]. Recently, cavity configuration-dependent pulse dynamics in KLM lasers [5–7] have been theoretically studied. Various bifurcations have been numerically predicted in specific configurations [5]. Regular, quasi-periodic and chaotic behaviors [6] have been obtained in a KLM laser at the edge of the stable region. By considering pulse propagation in both spatial and temporal domains, configuration-dependent period doubling, tripling, and quadrupling have been found in the KLM laser [7]. The dynamics involve the nonlinear modification of the spatial beam profile and temporal pulsewidth of the fundamental mode to vary the intensity. Similar dynamics, based on the iterative map of five variables, have also reported [8] to relate to some types of transition from stable to unstable regions, which depend on the unstable variable of chirp pulse in the KLM laser. Therefore, the KLM laser

* Corresponding author. Fax: +886-3-5712121ext56316.
E-mail address: wfhsieh@mail.nctu.edu.tw (W.-F. Hsieh).

0030-4018/$ - see front matter © 2003 Elsevier B.V. All rights reserved.
doi:10.1016/j.optcom.2003.07.044

is a favorable system for the study of nonlinear dynamics.

Experimentally, dynamic instability [9–11] in the soft-aperture KLM (SAKLM) Ti:sapphire laser also reveals dependence on the configuration of the cavity. By adjusting the separation between the two curved mirrors in a ring cavity near the edge of the stable region where is equivalent to a Fabry–Perot configuration, the behaviors of regular, period-doubling, quasi-periodic and chaotic states were observed [9]. Moreover, period doubling [10] and period-3 [11] pulses were observed when the X cavity configuration KLM Ti:sapphire lasers were at the confocal geometry and the 1/3-degenerate configuration. A general laser cavity is called 1/3-degenerace when its transverse frequency ($\Omega = \omega_0/\pi\cos^{-1}\sqrt{g_1 g_2}$) equals 1/3 of the longitudinal frequency ($\omega_0 = \pi c/L$) or $g_1 g_2 = 1/4$. For the soft-aperture Kerr-lens mode-locked laser, the pumping beam waist is smaller than the cavity beam waist within the gain medium such that the KLM mode which can self-reduce its beam size, due to self-focusing, to extract more energy from the inverted population, when the laser is operated near the degenerate cavity configuration. It has been used for optimizing the extraction efficiency of the solid-state lasers when the laser is operated near the degenerate configuration with tightly focused axial-pumping. In these configurations, the low order transverse modes may simultaneously be locked in the KLM laser, resulting in spatial sweeping of the beam profile at a frequency of Ω, which process has been called, "total mode locking" [11]. Furthermore, some hidden instabilities [12], caused by the variation of the spot size from pulse to pulse with a fixed pulse duration and energy, have been observed and explained by iterative maps [8]. However, no direct results of such experiments [9–12] elucidated the route to chaos in a KLM laser.

The three-frequency quasi-periodic route to chaos, called the Ruelle–Takens–Newhouse (RTN) route to chaos [13], has been reported in some laser systems, including the continuous wave (CW) operation of a gas He–Ne laser [14], a solid state Nd-YAG ring laser [15], and a mode-locking optical pumped NH_3 ring laser [16] which involves three modes within the gain bandwidth. As the active mode-locking external-cavity semiconductor laser exhibits multiple phase-locked longitudinal modes, the chaotic instability is a result of the nonlinear interaction among three periodic modes when the active mode-locking frequency is detuned from the cavity resonant frequency [17,18]. These modes are dynamic manifestations of the composite cavity resonance mode-locking frequency, the applied modulation, and the relaxation oscillation of laser [18].

Recently, the stable SAKLM was observed in degenerate cavity configurations [19], associated with the phase locking of the low-order degenerate transverse modes. Additionally, period doubling and period-3 pulses have been reported to occur around the 1/4-degeneracy (semi-confocal geometry) and 1/3-degeneracy with non-zero group velocity dispersion (GVD) [19], as predicted by the residue theorem [7]. The route from the quasi-periodic state to chaos when a KLM laser is operated near the zero GVD with the shortest pulses and the greatest nonlinearity has been described [20]. This route agrees quite well with the simulation result based on the Gaussian 4×4 matrix formalism, without considering transverse mode dynamics. In this work, the cavity is adjusted around the 1/3-degenerate configuration and the pumping power and the cavity configuration are chosen as the controlling parameters. A chaotic instability resulted from the interaction of three periodic frequencies in the SAKLM laser at trip GVD ~ -2500 fs^2. This paper is organized as follows. The next section describes the experimental setup for studying the nonlinear dynamics of the SAKLM laser. Section 3 presents the results and a discussion, covering the dynamic evolution of the laser pulses following variation of the pump power and cavity detuning. Detailed bifurcation diagrams and the various methods used to verify the determinism of the chaotic state are also presented. Finally, conclusions are drawn in Section 4.

2. Experimental

Fig. 1 depicts the experimental setup of a typical figure-Z SAKLM Ti:sapphire laser. An all-line CW argon ion laser (Coherent Innova 300) is

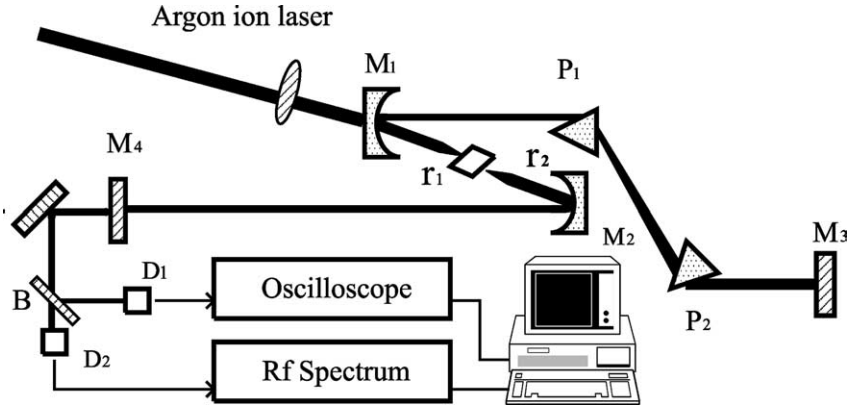

Fig. 1. Experimental setup of the SAKLM Ti:sapphire laser. D_1 and D_2 are high speed detectors and B is a beam splitter.

employed to pump the Ti:sapphire crystal via a plano-convex lens with a focal length of 12.7 cm. The laser cavity contains two curved mirrors, M_1 and M_2, both with radii of curvature of 10 cm and two flat mirrors, M_3 and M_4, as output couplers with 5% and 2% transmittance. A 9-mm long Brewster-cut Ti:sapphire laser rod is mounted between two curved mirrors at a distance r_1 from M_1 and r_2 from M_2. The distance from M_1 to M_3 is 75 cm and that from M_2 to M_4 is 74.5 cm. Consequently, the total length of the cavity is around 162 cm, corresponding to a repetition rate of 92.8 MHz. A pair of SF10 prisms (P_1 and P_2), separated by 27 cm, is inserted into the longer arm, M_1 to M_3, for GVD compensation. The total dispersion of the laser, which increases with the insertion depth of P_2, is operated at a round trip GVD ≈ -2500 fs^2 to generate the normal mode locking optical pulses as short as 80 fs [21]. This value is calculated by considering the negative GVD of the prisms [6] and the positive dispersion of the crystal. Two high-speed silicon p-i-n diodes with 500 ps rise time are used to detect the output optical signal; they are connected to a 300 MHz bandwidth digital oscilloscope (LeCroy 9450A) and an rf spectrum analyzer (HP-8560E).

As shown by our previous experimental work [19], SAKLM is usually operated near the fractional degenerate cavity configurations with peculiar mode patterns. These mode patterns can be decomposed as a superposition of the fundamental mode and degenerate low-order transverse modes. The laser is, thus, operated at around a 1/3-degeneracy or $g_1g_2 = 1/4$. Mechanically perturbing the laser causes it to enter a completely mode-locking (CML) state, consisting of a stable 10.8 ns regular pulse train without a CW component. The pump power was gradually increased and the dynamic evolution of the mode locking pulses and the corresponding spectra are recorded. The experiment was repeated by progressively reducing the pump power to determine whether the development of nonlinear dynamics is reversible. In addition, starting from the period-3 state [19], the mode locking states were recorded as the cavity configuration was varied by successively decreasing the separation between the two curved mirrors without changing the intra-cavity power too much.

3. Results and discussion

3.1. The pump power variation and the cavity length detuning induced pulse train dynamics

The pump power, P_p, was first chosen as the control parameter to observe the dynamic evolution when the cavity was slightly detuned from the 1/3-degenerate point. The laser system at $P_p = 4.5$ W was mechanically perturbed to cause the KLM of the laser, such that only a cavity resonant (or longitudinal) frequency of $f_1 = 92.8$ MHz was observed in the rf power spectrum of Fig. 2(a). In this state, no measurable fluctuation in the time

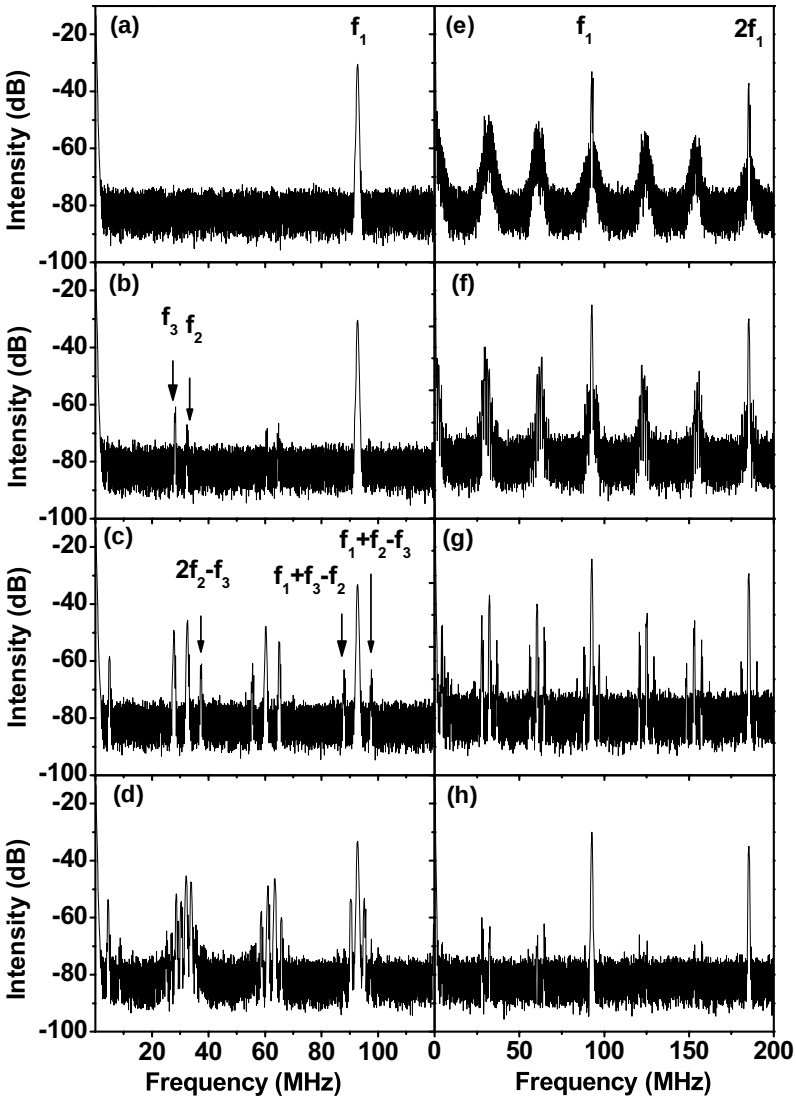

Fig. 2. Sequence of rf spectra variation, indicating the evolution of the dynamics as power increases with (a) in the complete mode-locked state with the longitudinal beat frequencies $f_1 = 92.8$ MHz, (b) in the quasi-periodic state with the generation of two additional frequencies, (c) for a combination tones occurring, (d) in a quasi-periodic spectrum with secondary beatings, (e) in the chaotic state on a coarse scale, and the evolution as the power declines, as shown in (f)–(h).

sequence and so the state is referred to as the CML state. As the pump power was increased to 5 W, four beatings were generated below the longitudinal beating frequency, f_1, in Fig. 2(b). They are 32.2 MHz, labeled f_2, accompanied by a 3.8 MHz down-shift beat frequency, f_3, at 28.4 MHz as well as the other frequencies at around 2/3 f_1. The 3.8-MHz frequency was checked not to result from plasma oscillations in the Ar^+ laser to induce gain modulation in the Ti:sapphire. Furthermore, the same nonlinear dynamics were observed in the Ti:sapphire laser when a frequency doubling Nd:YVO_4 laser (Coherent, Verdi-V8) was used as the pumping source.

As P_p was further increased to 6.2 W, additional beating frequencies were observed at $2f_2 - f_3$, $f_1 + f_3 - f_2$ and $f_1 + f_2 - f_3$, as shown in Fig. 2(c). These beatings are due to the third-order nonlinear interaction, which induces four-wave mixing [15] of the optical waves at three periodic frequencies $v_0 \pm nf_1$, $v_0 \pm nf_1 \pm f_2$, and $v_0 \pm nf_1 \pm f_3$ in the active medium under high intra-cavity power. Here v_0 is the specific optical frequency of a longitudinal mode. When $P_p = 6.9$ W, nonlinear interaction strengthens accordingly, and the secondary beatings generated by the combination tones oscillate all together, broadening the spectrum as shown in Fig. 2(d). Finally, a quasi-continuum spectrum was generated at $P_p = 7.7$ W, indicating that the dynamic system had an aperiodic attractor. Fig. 2(e) shows an rf spectrum, on a coarse frequency scale displays to show the second longitudinal beating. The broadened spectrum exhibits exponential decay or linear decay on the dB scale, not only around the longitudinal beatings but also around the 1/3 and 2/3 longitudinal frequencies. As the pump power was reduced, the quasi-periodic spectrum with secondary beatings emerged at $P_p = 7.2$ W again in Fig. 2(f). The quasi-periodic state with three major peaks around the longitudinal frequency as well as the 1/3 and 2/3 longitudinal frequencies are seen in the power spectrum of Fig. 2(g) at $P_p = 6.5$ W which is equivalent to that in Fig. 2(c). The dynamics recovered to the three-frequency quasi-periodic state as the pumping power was declined to 6.0 W, as shown in Fig. 2(h). Finally, all of the beatings, except the longitudinal ones, disappeared as the pump power was tuned below 5 W.

The cavity length was chosen as the control parameter by shortening the distance r_2, to investigate the cavity configuration-dependent dynamics of the SAKLM laser. In this experiment, the laser cavity length was adjusted at the 1/3-degeneracy at $P_p = 5$ W, to obtain the period-3 state, whose power spectrum in Fig. 3(a) shows two beatings at 1/3 (f_2) and 2/3 of the longitudinal frequency f_1 ($f_1 = 92.8$ MHz). As r_2 was shortened by 20 μm, the abrupt down-shift of the beat frequency f_2 to 23 MHz was accompanied by the appearance of another frequency $f_3 = 47.7$ MHz in Fig. 3(b). In Fig. 3(c), the beat frequencies f_2 and f_3 moved closer together, as in the quasi-periodic state in Fig. 2(b), when the cavity length was reduced by 10 μm. Shortening r_2 by another 20 μm caused the third-order nonlinearity-induced four-wave mixing caused the combination tones $2f_2 - f_3$, $2f_3 - f_2$, $f_1 + f_2 - f_3$ and $f_1 + f_3 - f_2$ to appear in Fig. 3(d). Then, each characteristic beating in the spectrum was broadened, as shown in Fig. 3(e) when r_2 was shortened by another 20 μm. Finally, the system became chaotic, with its power spectrum broadened over a very wide range of frequencies, as shown in Fig. 3(f), when the cavity was shortened by an additional 30 μm. The observation of the development from the period-3 through the quasi-periodic state to chaos, when the cavity configuration was tuned slightly away from degeneration in this experiment, could be related to the reduction in the bifurcation threshold, as predicted previously [7,22].

3.2. Bifurcation diagram

Figs. 4(a) and (b) show bifurcation diagrams of the beat frequencies versus the pump power and cavity length, respectively, to clarify how the system transforms from a system in a periodic state to one in chaos. Unsurprisingly, the longitudinal frequency (labeled f_1) is essentially constant throughout the variation of the pump power and the detuning of the length of the cavity. When the pump power increases or the length of the cavity is detuned further, the beat frequencies, f_2 and f_3, are tuned slightly away from 1/3 f_1, as shown in Figs. 4(a) and (b). The further detuning of the configuration from the 1/3-degeneracy may have been due to the Kerr nonlinearity and the thermal lens effect at high pumping power in this experiment. Notably, the frequency f_2 near $1/3f_1$, marked by a horizontal bar, exhibits no obvious shift, regardless of the pump power or the configuration. However, the combination tones are duplicated through four-wave mixing in the active medium, when pump power increases within $5.3\ \text{W} < P_p < 6.8$ W or the cavity is shortened. Then, the satellite peaks develop and become wider as the combination tones undergo nonlinear wave mixing when the pump power exceeds 6.8 W or the cavity

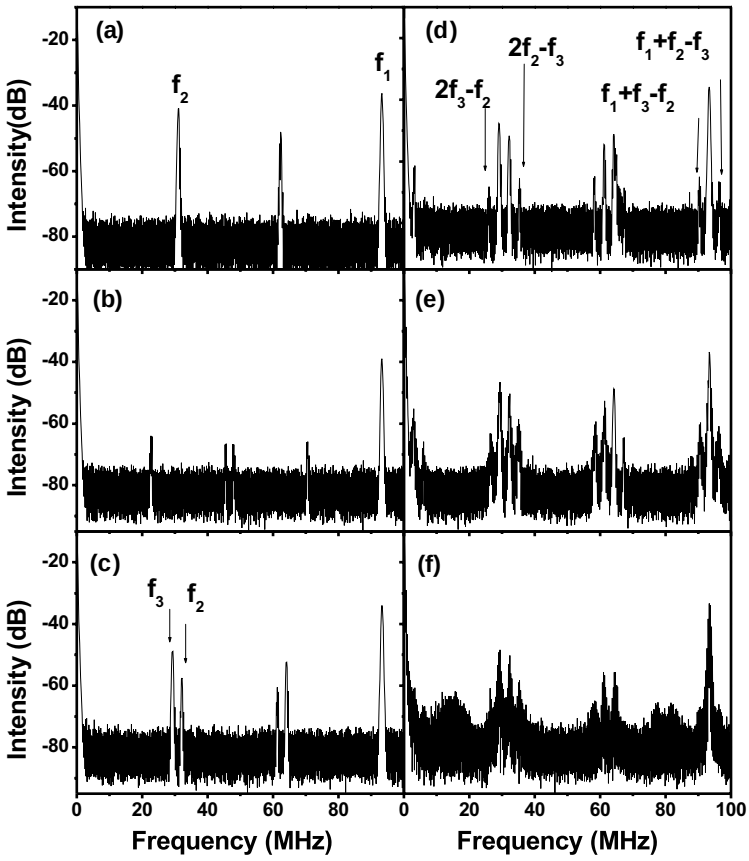

Fig. 3. Sequence of rf spectra variation, showing the evolution from the period-3 state to chaos as the configuration is varied with (a) in a period-3 state, (b) and (c) in a quasi-period state with the generation of two additional frequencies, (d) with a combination tones occurring, (e) with spectrum broadening and (f) in a chaotic state.

is shortened further; accordingly, the system finally becomes chaotic.

The bifurcation behaviors mentioned above are similar to the simulated behaviors obtained by considering the gain saturation as the only nonlinear effect under good cavity conditions (cavity loss per round trip $<10\%$) in an axially pump laser with a simple cavity [22]. The Huygens diffraction integral and the rate equation are used to yield a V-shaped quasi-periodic threshold near the 1/3-degenerate cavity configuration when the radius of the pump beam exceeds that of the cavity beam. As the configuration is shifted slightly away from degeneracy, the laser enters chaos because of the interplay between beam propagation and gain dynamics. Furthermore, the bifurcation that occurs as the pump power increases was also been obtained in this simulation result, causing the system finally to enter chaos near degeneracy.

The generation of two beat frequencies at one-third and two-thirds of f_1 in Fig. 4(b) (period-3 pulses) could have resulted from transverse mode locking [10,11] if other non-degenerate TEM_{01} (or TEM_{10}) modes are simultaneously phase-locked to the TEM_{00} modes. A simple calculation indicates that the shift in the frequency of the TEM_{01} modes from $1/3\omega_0$ and the shift in the frequency of the TEM_{03} mode relative to the TEM_{00} mode are approximately 1 and 2–3 MHz, respectively, when a 100 μm cavity is detuned away from 1/3-degeneracy. However, as shown in the bifurcation of Fig. 4, a constant value of f_2 was experimentally

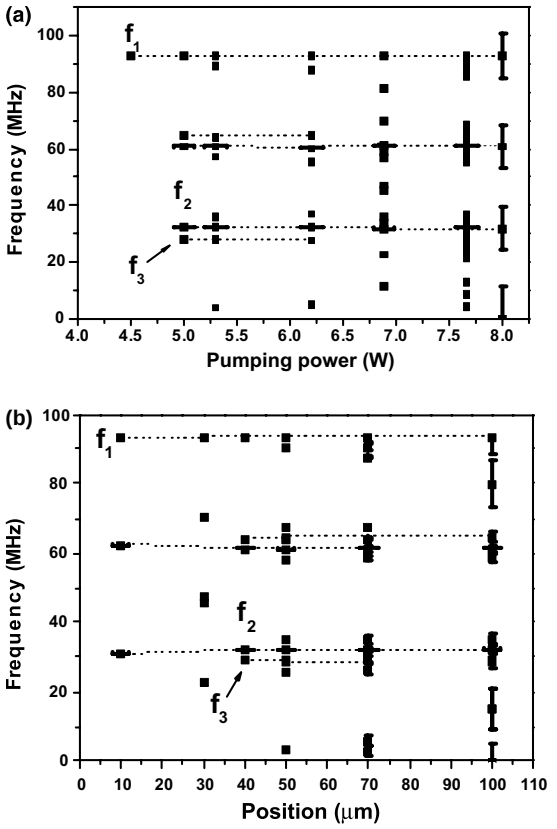

Fig. 4. Bifurcation diagram obtained by taking (a) the pumping power, (b) and the detuning of the configuration as the control parameter.

observed throughout the variation of the pump power and the detuning of the cavity. Therefore, the transverse mode locking may not be the reason to result in the dynamic instability in our laser system. Additionally, the dynamics of the CW and KLM lasers in terms of the q-parameter have been theoretically studied [7,22–25]. In particular, Sanchez and Hnilo [24,25] analyzed the general conditions for the periodic solutions. The circulation of the fundamental mode with n discrete dots in the phase space (W, W/R) for $1/n$-degeneracy can also be expressed in terms of the q-parameter [7,22,23]. Therefore, the period-3 state was the theoretically predicted in the 1/3-degenerate configuration for $n = 3$. The quasi-periodic route to chaos by cavity detuning is consistent with the simulation results [22], which indicate that the instability threshold of the laser is lower when the configuration is tuned slightly away from degeneracy.

The quasi-periodic route to low-dimensional chaos in the KLM laser around zero GVD, due to the shortest pulses than the pulses within other GVD regime to result in the highest nonlinearity, has been well explained by the Gaussian 4×4 matrix without considering the transverse mode effect [20]. In contrast, for a round trip GVD of -2500 fs^2, experiments reveal period-3 and irregular pulse behaviors around the 1/3-degenerate configuration [19]. These findings agree closely with the theoretical prediction of the KLM instability around 1/3-degeneracy of the SAKLM laser when the Kerr effect is considered to be the source of nonlinearity [7]. In this simulation, self-focusing and self-phase modulation are taken into account in both spatial and temporal domains, when an ultra-short pulse travels through a Kerr medium. An iterative map that includes the parameters of spot size, curvature, pulsewidth and frequency chirping around a round trip GVD of 2560 fs^2 shows that period-3 pulses are generated and reveals the three different spot sizes and pulsewidths in order. Irregular variations in intensity are observed when the Kerr parameter K exceeds 0.4.

3.3. Nonlinear dynamic analysis

The measured data in the laser dynamic experiment are continuous or represent a discrete time sequence of laser outputs $x(t)$, recorded by an electronic instrument (such as an oscilloscope) with a sampling interval of τ, and represented by $x(\tau_0 + n\tau)$ or x_n. A return map plotted by x_n and x_{n+1} can be used to construct the phase portrait and display the points of intersection of the trajectory with a definite surface. For a pulsed output laser, with the data of a discrete time sequence, the peak detection return map of $I(n)$ versus $I(n+1)$ obtained from the recorded temporal pulse traces is used to avoid some confusion with the data from the CW state, as shown in Fig. 5. Indeed, a "thick" closed loop phase plot in Fig. 5(a) represents the quasi-period state (Fig. 2(h)), with a trajectory that moves on a torus in phase space. The diffused return map in Fig. 5(b) implies that the spectrum-broadened state of the

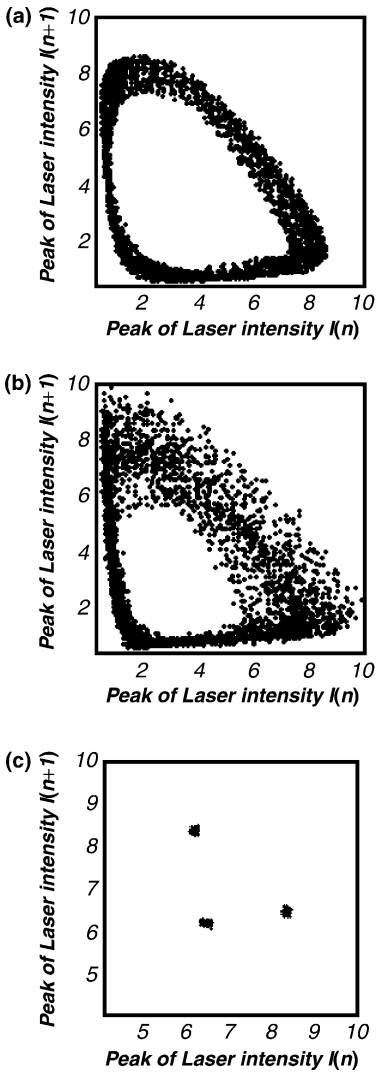

Fig. 5. Peak detection return map for the (a) quasi-periodic, (b) chaotic and (c) period-3 states.

laser in Fig. 2(e) is chaotic. The return map of the period-3 state in Fig. 5(c) clearly shows three groups of data points.

Although the power spectrum, obtained directly from the Fourier transform of the measured time sequence, reveals a broad continuum for a system in chaotic state, the stochastic signal exhibits a similar feature, as well as the fluctuating trace and diffused return map. The autocorrelation of pulses may also provide some information on whether the system is chaotic, that does not decay in the periodic and quasi-periodic state but decays immediately if the signal is noise. In the chaotic state, the autocorrelation of pulses exponentially decays. The autocorrelation calculated from the time traces of pulses with a little decay in Fig. 6(a) confirms that Fig. 3(c) is quasi-periodic. The exponential decline of the autocorrelation with a long decay time in Fig. 6(b) verifies a broadened spectrum in Fig. 3(f) at the weak chaotic state.

Moreover, noise has infinitely dimensional in contrast to the chaotic signal has a fractal low dimensional attractor. However, the experimentally measured time sequence x_n contains information on several dynamical variables, projected into one dimension, and therefore cannot completely describe the system. The time embedding technique is required to reconstruct the trajectory in D_e-dimensional "embedding space" from the time series to determine quantitatively the fractal characteristic of the nonlinear dynamic attractor by calculating its correlation dimension using the Grassberger–Procaccia analysis (GPA) [26,27]. The calculated correlation dimension for the

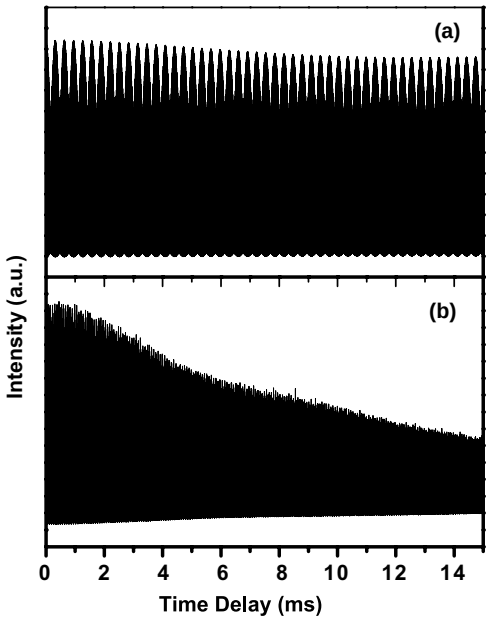

Fig. 6. Autocorrelation of pulses in the (a) quasi-periodic and (b) chaotic states.

dynamical variable x_n increases with the embedding dimension D_e, finally reaching a constant when the D_e is sufficiently large to accommodate the attractor. The commercial chaos data analyzer (CDA) from the American Institute of Physics was used to analyze our data (for example, in Fig. 2(e)). Each mode locking pulse containing around 5–6 points and a total of 3500 pulses acquired by our oscilloscope are used for this calculation. Each data point represents an accumulation of time interval over approximately 2 ns. The maximum value of the voltage on the oscilloscope, with 8-bit flash, is read as approximately 2 V for our measured pulse train. The 3500 acquired mode-locking pulses without peak detection were used directly to calculate the embedding dimension. The correlation dimension for our measured pulse trains is independent of the peak detection data used. The convergent low fractal dimension of around three, labeled by the square in Fig. 7(a), implies that the random-looking oscillation is deterministic, excluding the possibility that the instability is due to noise.

The false nearest-neighbors (FNN) [28] analysis could also help to establish the chaotic nature of the signal and discriminate it from noise. Fig. 7(b) presents the results of the FNN analysis of the chaotic data (square dots), revealing a rapid fall to zero at a low embedding dimension of around seven. Nevertheless, the FNN for the x_n from random noise declines to a non-zero value and rises again as D_e increases. Surrogate data [29] are produced by Fourier-transforming the original data, randomizing the phase and then reverse-Fourier-transforming them back, to check further the determinism of the data. The new set of data resembles the original set data but lacks the determinism. The surrogate data are then analyzed by the GPA and the FNN analysis whose results are shown by circles in Figs. 7(a) and (b). The absence of convergence, indicated by large error bars in the calculation of the correlation dimension, and the offset value from zero at a high embedding dimension in the FNN analysis further confirm that the irregular pulse behavior is chaotic. According to the Takens and Mane theorems, the embedding dimension D_e and the dimension n of a manifold that contains an attractor must

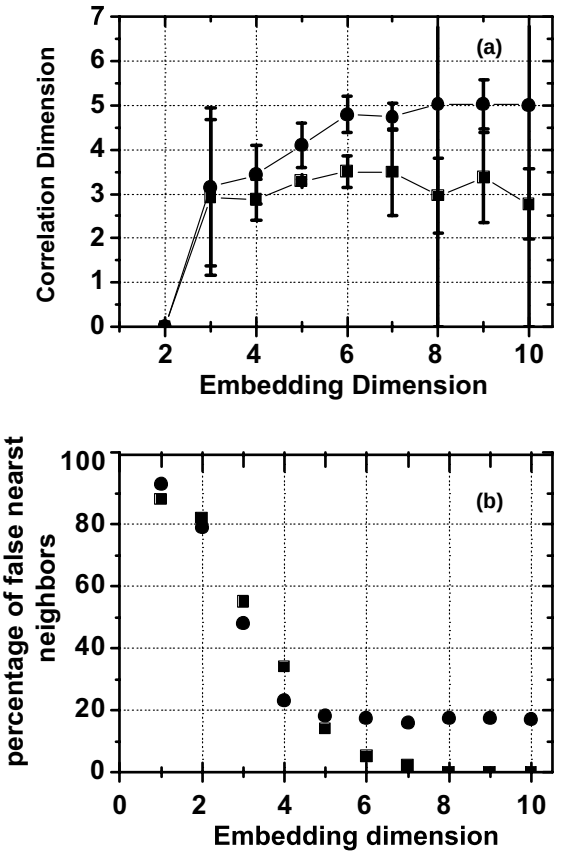

Fig. 7. The (a) correlation dimension and (b) false nearest-neighbors versus the embedding dimension for the chaotic data (squares) and its surrogate data (circles).

satisfy the inequality $D_e \geqslant 2n+1$ (the so-called "Takens criterion"). The value of the calculated correlation dimension from our acquired chaotic SAKLM time series converges to around three ($n=3$) when the embedding dimension D_e exceeds 7. Furthermore, a declining of the FNN to zero is approached as the embedding dimension approaches seven that reveals the minimum value needed to unfold the attractor from the measured time series. The result is consistent with the Takens criterion $D_e \geqslant 2n+1=7$.

4. Conclusion

Period-3 pulses and irregular chaotic behavior are experimentally observed within a non-zero

GVD regime in a SAKLM Ti:sapphire laser in around the 1/3-degenerate configuration. The dynamics follow mainly from the three-periodic frequency interaction among the longitudinal frequency and the other two additional frequencies, close to one-third of the longitudinal frequency. The details of the bifurcation, including the combination tones and further secondary beatings were experimentally observed before the chaotic state was entered as pumping was increased. This quasi-periodic route to chaos from the three-frequency interaction around the 1/3-degenerate cavity configuration of the soft-aperture Kerr-lens mode-locked Ti:sapphire laser is observed with non-zero group velocity dispersion similar to the condition used in our previous simulation. Beginning with period-3 pulses, a similar evolution to chaos due to a three-frequency interaction was found by reducing the length of the cavity, r_2. Finally, the chaotic state was verified via the diffused return map of the measured pulses after the peak-detection and the exponential decay autocorrelation function of the pulse trains. The calculated non-integer correlation dimensions of around three for the chaotic signal were in contrast to the surrogate data with a non-convergent correlation dimension. Furthermore, the rapidly decline to zero of the chaotic signal, according to FNN analysis contrast with the non-zero value of surrogate data further demonstrates the determinism of the data.

Acknowledgements

The authors are grateful for useful discussions with Prof. Ming-Dar Wei at Feng-Chia University, Taiwan. This work was partially supported by the National Science Council (NSC) and the Ministry of Education of the Republic of China under Grants NSC91-2112-009-040 and 90-E-6-FA-1-4. Mr. Ja-Hon Lin would like to thank NSC for the award of his fellowship.

References

[1] D.E. Spence, P.N. Kean, W. Sibbett, Opt. Lett. 16 (1991) 42.
[2] K.-H. Lin, W.-F. Hsieh, J. Opt. Soc. Am. B 11 (1994) 737.
[3] K.-H. Lin, Y. Lai, W.-F. Hsieh, J. Opt. Soc. Am. B 12 (1995) 468.
[4] K.-H. Lin, W.-F. Hsieh, J. Opt. Soc. Am. B 13 (1996) 1786.
[5] M.-D. Wei, W.-F. Hsieh, Opt. Commun. 168 (1999) 161.
[6] V.L. Kalashnikov, I.G. Poloyko, V.P. Mikhailov, J. Opt. Soc. Am. B 14 (1997) 2691.
[7] M.-D. Wei, W.-F. Hsieh, J. Opt. Soc. Am. B 17 (2000) 1335.
[8] M.G. Kovalsky, A.A. Hnilo, Opt. Commun. 186 (2000) 155.
[9] Q. Xing, L. Chai, W. Zhang, C.-Y. Wang, Opt. Commun. 162 (1999) 71.
[10] D. Cote, H.M. van Driel, Opt. Lett. 23 (1998) 715.
[11] S.R. Bolton, R.A. Jenks, C.N. Elkinton, G. Sucha, J. Opt. Soc. Am. B 16 (1999) 339.
[12] M.G. Kovalsky, Alejandro A. Hnilo, Carlota M.F. Gonalez Inchauspe, Opt. Lett. 24 (1999) 1638.
[13] S. Newhouse, D. Rulle, F. Takens, Commun. Math. Phys. 64 (1978) 35.
[14] N.J. Halas, S.N. Liu, N.B. Abraham, Phys. Rev. A 28 (1983) 2915.
[15] F. Hollinger, Chr. Jung, H. Weber, Opt. Commun. 75 (1990) 84.
[16] D.Y. Tang, M.Y. Li, N.R. Heckenberg, U. Hubner, J. Opt. Soc. Am. B 13 (1996) 2055.
[17] B.C. Lam, A.L. Kellner, M.M. Sushchik, H.D.I. Abarbanel, P.K.L. Yu, J. Opt. Soc. Am. B 10 (1993) 2065.
[18] B.C. Lam, M.M. Sushchik, H.D.I. Abarbenel, A.L. Kellner, P.K.L. Yu, J. Opt. Soc. Am. B 12 (1995) 1150.
[19] J.-H. Lin, M.-D. Wei, W.-F. Hsieh, H.-H. Wu, J. Opt. Soc. Am. B 18 (2001) 1069.
[20] S.R. Bolton, M.R. Acton, Phys. Rev. A 62 (2000) 063803-1.
[21] J.H. Lin, W.F. Hsieh, H.H. Wu, Opt. Commun. (2002) 149.
[22] C.H. Chen, M.D. Wei, W.F. Hsieh, J. Opt. Soc. Am. B 18 (2001) 1076.
[23] M.D. Wei, W.F. Hsieh, C.C. Sung, Opt. Commun. 146 (1998) 201.
[24] L.M. Sanchez, A.A. Hnilo, Opt. Commun. 166 (1999) 229.
[25] L.M. Sanchez, A.A. Hnilo, Opt. Commun. 199 (2001) 189.
[26] P. Grassberger, I. Procaccia, Phys. Rev. Lett. 50 (1983) 346.
[27] A. Ben-Mizrachi, I. Procaccia, P. Grassberger, Phys. Rev. A 29 (1984) 975.
[28] M.B. Kennel, R. Brown, H.D.I. Abarbanel, Phys. Rev. A 45 (1992) 3403.
[29] J. Theiler, S. Eubank, A. Longtin, B. Galdrikian, J.D. Farmer, Physica D 58 (1992) 77.